



HAL
open science

Electrical Resistivity-Based Approach to Characterize Moisture Content in Compressed Earth Bricks

Tuan Anh Nguyen, Minh Dung Pham, Wael Hafsa, Nicolas Angellier, Laurent
Ulmet, Frédéric Dubois

► **To cite this version:**

Tuan Anh Nguyen, Minh Dung Pham, Wael Hafsa, Nicolas Angellier, Laurent Ulmet, et al.. Electrical Resistivity-Based Approach to Characterize Moisture Content in Compressed Earth Bricks. Case Studies in Construction Materials, 2024, 21, pp.e04027. 10.1016/j.cscm.2024.e04027 . hal-04802249

HAL Id: hal-04802249

<https://hal.science/hal-04802249v1>

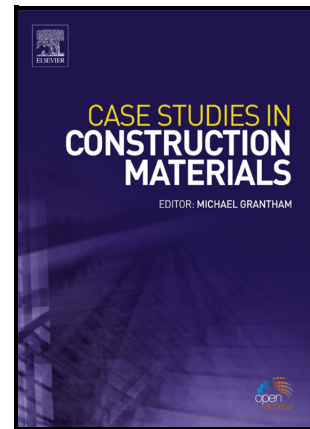
Submitted on 3 Dec 2024

HAL is a multi-disciplinary open access archive for the deposit and dissemination of scientific research documents, whether they are published or not. The documents may come from teaching and research institutions in France or abroad, or from public or private research centers.

L'archive ouverte pluridisciplinaire **HAL**, est destinée au dépôt et à la diffusion de documents scientifiques de niveau recherche, publiés ou non, émanant des établissements d'enseignement et de recherche français ou étrangers, des laboratoires publics ou privés.

Electrical Resistivity-Based Approach to Characterize Moisture Content in Compressed Earth Bricks

Tuan Anh NGUYEN, Minh Dung PHAM, Wael HAFSA, Nicolas ANGELLIER, Laurent ULMET, Frédéric DUBOIS



PII: S2214-5095(24)01179-3

DOI: <https://doi.org/10.1016/j.cscm.2024.e04027>

Reference: CSCM4027

To appear in: *Case Studies in Construction Materials*

Received date: 13 March 2024

Revised date: 9 November 2024

Accepted date: 22 November 2024

Please cite this article as: Tuan Anh NGUYEN, Minh Dung PHAM, Wael HAFSA, Nicolas ANGELLIER, Laurent ULMET and Frédéric DUBOIS, Electrical Resistivity-Based Approach to Characterize Moisture Content in Compressed Earth Bricks, *Case Studies in Construction Materials*, (2024) doi:<https://doi.org/10.1016/j.cscm.2024.e04027>

This is a PDF file of an article that has undergone enhancements after acceptance, such as the addition of a cover page and metadata, and formatting for readability, but it is not yet the definitive version of record. This version will undergo additional copyediting, typesetting and review before it is published in its final form, but we are providing this version to give early visibility of the article. Please note that, during the production process, errors may be discovered which could affect the content, and all legal disclaimers that apply to the journal pertain.

Electrical Resistivity-Based Approach to Characterize Moisture Content in Compressed Earth Bricks

Tuan Anh NGUYEN^{1*}, Minh Dung PHAM², Wael HAFSA³, Nicolas ANGELLIER⁴,
Laurent ULMET⁴ and Frédéric DUBOIS⁴

*Abstract

Compressed earth bricks (CEBs) are increasingly used as a sustainable building material, but their hygroscopic nature makes them susceptible to moisture-related degradation. Monitoring moisture content in CEBs is crucial for ensuring structural integrity and durability, yet existing methods are often destructive or limited in application. This study presents a non-destructive approach for assessing moisture content in CEBs using electrical resistivity measurements, adapted from geophysical surveying techniques. The research employed a modified Syscal Junior Switch-48 resistivity meter with 4-electrode and 16-electrode configurations to measure electrical resistance in CEB samples under controlled relative humidity conditions ranging from 20% to 100%. Clear logarithmic correlations were established between moisture content (1.86-9.48%) and electrical resistivity. The measured electrical resistivity varied from 12.4Ωm at 9.48% moisture content to 3350Ωm at 1.86% moisture content, demonstrating the method's sensitivity across a wide range of moisture levels. The 50mA measurement mode demonstrated capability to assess moisture levels down to 1.86%, while the standard 1250mA mode was effective above 2.9% moisture content. Numerical modeling using finite element analysis was conducted to determine geometric factors and true resistivity values. The 16-electrode multiplexed measurements showed good agreement with the experimental trend, enabling potential internal moisture mapping. This application of resistivity measurements represents a significant advance in non-destructive monitoring of earthen construction materials.

Keywords: Compressed Earth Bricks, Moisture monitoring, Electrical resistivity measurements, Hygroscopic material.

1. Introduction

The growing environmental concerns have instigated a pursuit for alternative solutions within the civil engineering sector, with a focus on prioritizing the utilization of natural materials. Among these solutions, the utilization of natural materials such as wood and earth material has gained significant

¹ BRIDGE Research Group, Ho Chi Minh City University of Transport, Vietnam

*Corresponding author

² Vietnam Institute of Architecture

³ Aix-Marseille University, CNRS IUSTI UMR 7343, France

⁴ Civil Engineering Laboratory, Diagnostic and Sustainability (GC2D), University of Limoges, France

attention. These materials have a rich historical precedent and have proven their durability over time, making them a promising option for sustainable construction practices [1-4].

Earth material, specifically, emerges as one of the most ancient natural building resources that has enjoyed favour with humanity since the dawn of prehistoric eras. Remarkably, at present, approximately one-third of the global population resides in domiciles fashioned from earth-based construction methods, encompassing diverse techniques such as rammed earth, adobe bricks, and compressed blocks [1, 5, 6]. The enduring prevalence of earth material construction serves as a testament to its exceptional attributes and its compatibility with sustainable construction practices. Earth material possesses a multitude of advantageous characteristics that designate it as an environmentally-conscious and sustainable construction medium [3, 6-10]. Notably, its production demands minimal energy when compared with materials like concrete or steel, thereby concomitantly mitigating associated carbon emissions and aligning with the principles of sustainable development [2]. Furthermore, earth material is highly recyclable and can be easily reintegrated into the environment without adverse ecological repercussions. This inherent quality significantly curtails waste generation, aligning seamlessly with the tenets of the circular economy, which places paramount importance on resource efficiency.

One of the notable techniques in the field of construction is the utilization of Compressed earth bricks (CEBs) [11-13]. Among these techniques, the extrusion manufacturing method has gained attention due to its high production speed and repeatability. Similar to other construction materials derived from earth, CEBs possess hygroscopic properties, which enable them to absorb and release moisture from the surrounding environment [7, 14-18].

CEBs exhibit a remarkable ability to absorb moisture from their surroundings, allowing for the regulation of indoor humidity levels and contributing to a healthier, more comfortable living environment. According to Laou's research [19], which employed a numerical model simulating the hygro-thermo-mechanical behavior of earth bricks over a one-year period in a T4-type house (comprising a living room, three bedrooms, kitchen, bathroom, and toilet), and accounting for fluctuations in indoor and outdoor temperature and moisture levels, earth brick partition walls demonstrated superior performance in maintaining hygrometric comfort compared to traditional plaster walls. This comprehensive study, which incorporated experimentally determined thermal, hygroscopic, and mechanical properties of earth bricks into the model, effectively highlighted the material's remarkable ability to regulate indoor humidity. However, this hygroscopic nature presents challenges. Excessive moisture absorption can lead to decreased mechanical strength in the bricks, potentially causing cracking and deformation. Laou et al. [20] conducted research to establish the scientific basis for predicting the hygroscopic and mechanical behaviour of CEBs as a function of relative humidity, which is a key factor in controlling indoor comfort. Their study affirmed that, alongside factors such as the $\text{SiO}_2/\text{Al}_2\text{O}_3$ ratio, the porosity rate, the pore size distribution, the nature of the clay minerals, moisture content is one of the critical factors influencing the performance of these bricks. Therefore, the monitoring of moisture content plays a significant role in ensuring the quality and durability of structures constructed with CEB [18, 21, 22].

Despite the importance of moisture content in CEBs, there is a notable scarcity of research on non-destructive methods for its determination. Currently, the primary method for measuring moisture content in CEBs is the weighing method, which is destructive and thus limited in its

application to existing structures. Non-destructive testing (NDT) methods have been extensively researched and applied to CEBs, but these studies have predominantly focused on other characteristics such as chemical composition, density, and mechanical properties. X-ray methods have been used for compositional analysis [23-25], while ultrasonic techniques have assessed density and mechanical properties like compressive strength and dynamic modulus [4, 26, 27]. Navaratnarajah et al. [28] combined ultrasonic pulse velocity and electrical resistivity to qualitatively evaluate cement-stabilized earth blocks. However, the application of NDT methods specifically for moisture content determination in CEBs remains notably scarce, creating a significant research gap. Given the importance of moisture content in influencing the performance and durability of these earth-based construction materials, developing non-destructive methods for moisture content assessment in CEBs is not only necessary but could be considered a pioneering direction in sustainable construction research.

Electrical methods have been applied to assess the moisture content of CEBs, leveraging the conductive properties of water within the material. Elisabete R. T. [29] et al. extended the application of the electrical method to evaluate moisture-related characteristics of CEB by measuring the electrical resistivity of CEB bricks at various moisture levels. However, this study primarily focused on assessing water permeability at high moisture levels, while at lower moisture levels, when CEBs have higher resistivity, there is still a need for an accurate and non-destructive measurement method.

A promising approach was implemented by Hafsa et al. [30] in the field of hygroscopic materials. The study employed the Electrical Resistivity Tomography (ERT) method [31, 32] to assess moisture content in Douglas-fir wood. This method, adapted from a widely used technique in geophysical surveys, successfully established a correlation between moisture content and electrical resistivity in wood. ERT allows for measuring the distribution of electrical resistivity within a material sample to infer its moisture content, without causing any damage to the material. This method has proven to lay the foundation for the initial success of applying the ERT method to wood (a material with higher electrical resistivity than CEBs). The success of ERT in assessing moisture content in wood - another hygroscopic material - suggests that this method could be effectively applied to CEBs. However, to date, no study has applied ERT to assess moisture content in CEBs. This represents a significant research gap in the field.

This study demonstrates the potential for applying the previously established electrical resistivity technique to characterize moisture-dependent properties of CEB. The aim of the research was to examine the appropriateness and efficacy of the electrical method for non-destructive moisture content assessment in CEB materials. This paper begins by introducing the theoretical basis of the electrical resistivity method and its application for moisture measurement. The experimental section then describes the materials, equipment, and protocols for electrical testing using both standard 4-electrode and multiplexed configurations. Subsequently, the numerical modelling approach is presented, simulating the experiments through finite element analysis. Finally, the results are analyzed comprehensively, key findings discussed, and conclusions drawn regarding the efficacy of the electrical method for non-destructive moisture evaluation of compressed earth bricks.

2. Principle and theoretical background of the electrical resistivity method

The similarity of Ohm's, Fick's laws underscore the correlation between electrical and heat transfer phenomena. These laws further demonstrate a direct proportionality between the effects,

such as mass flux density, current density, and their respective causes, namely the potential gradient or particle density. Table 1 provides a summary of the similarities between electrical and heat transfer [33].

Table 1. Analogies between electrical, mass and heat transfer [33]

Transport analogies	Electrical (e)	Heat (Q)
Flux (current density)	\vec{j}_e	\vec{j}_Q
Characteristics variable	Electric potential φ	Temperature θ
Driving force	Electric potential gradient $\nabla\varphi$	Temperature gradient $\nabla\theta$
Proportionality factor	Electrical conductivity κ_e	Thermal conductivity κ_Q

The Electrical Resistivity Method is a geophysical technique widely employed in the field. Its foundation lies in generating an electrical potential difference (voltage) around current-carrying electrodes embedded in a conductive medium. The voltage distribution around subsurface-driven current electrodes is contingent upon the electrical resistivities of the subsurface materials and their spatial variations.

This method involves introducing electrical current into the subsurface using two current electrodes and simultaneously measuring the resulting potential difference across two potential electrodes. Each resistivity measurement requires the use of four electrodes grounded to the subsurface, providing the apparent resistivity of the materials situated between the potential electrodes. Resistivity surveys typically deploy multiple electrode pairs arranged in various spatial geometries, selected based on site-specific parameters and/or the objectives of the survey.

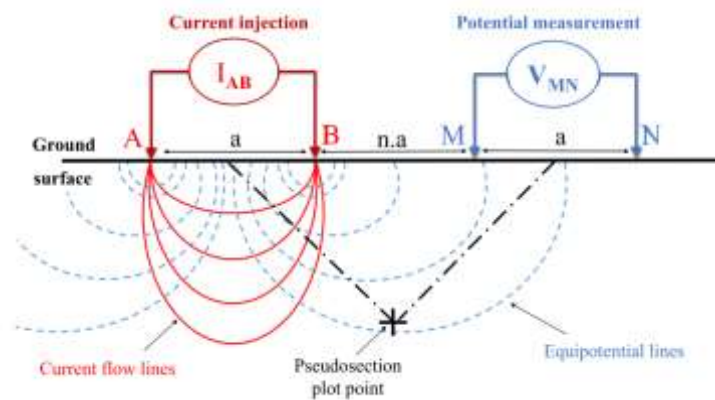


Figure 1. Schematic representation of a 1D Dipole-dipole array

In scenarios involving a homogeneous and isotropic medium, the resistivity observed can be equated to the true resistivity. However, when dealing with heterogeneous environments, this

assumption no longer holds. In such cases, the concept of apparent resistivity is introduced as a means of characterizing and understanding the electrical behavior of the subsurface [29, 32].

For instance, as illustrated in Figure 1, the methodology for evaluating subsurface resistivity involves a systematic deployment of four electrodes in the ground. In this arrangement, a precisely measured direct current or low-frequency alternating current is applied between electrodes A and B, denoted as $I_{AB}(A)$. Following this, the resulting alternating current voltage $\Delta V_{MN}(\Omega)$ is measured between electrodes M and N, which are designated as potential electrodes.

The apparent resistivity is defined by:

$$\rho_{app} = K \frac{\Delta V_{MN}}{I_{AB}} \quad (1)$$

ρ_{app} : apparent resistivity (Ωm)

The geometric factor K is calculated using the following formula:

$$K = \frac{2\pi}{\left(\frac{1}{AM} - \frac{1}{BM}\right) - \left(\frac{1}{AN} - \frac{1}{BN}\right)} \quad (2)$$

AM, BM, AN, BN are the corresponding distances between electrodes.

In the context of electrical transmission within a finite medium, the calculation of the geometric factor deviates from the application of formula (2), which is derived under the assumption of electrical transmission in a semi-infinite medium environment. The geometric factor, denoted as K_m needs to be adjusted to account for both the measurement configuration and the finite nature of the electrical transmission medium of the test sample. K_m not only depends on the quadrupole type and the distance between electrodes but also varies based on the shape of the object being measured. In this case, the apparent resistivity is calculated using the following formula:

$$\rho_{app} = K_m \frac{\Delta V_{MN}}{I_{AB}} \quad (3)$$

3. Experimental Protocol

3.1. Material

The bricks used in this study were obtained from a brick factory located in the Southwest of France. These bricks, with dimensions of $225 \times 110 \times 50 \text{mm}^3$, are formed through the process of vacuum extrusion. The extrusion process introduces a certain level of anisotropy, resulting from the orientation of the clay sheet. As a consequence, the hydric, thermal, and mechanical properties of the bricks exhibit variations in two distinct directions: perpendicular and parallel to the extrusion direction [14], [35].

This type of brick has been studied by Lamyaa Laou [24] revealing the following characteristics:

- The chemical compositions of the mixtures used in brick manufacturing are determined by chemical analysis using X-ray fluorescence data, as presented in the following table. The

obtained fire loss can be attributed, on the one hand, to the capillary retention of the material and the dihydroxylation of the phyllosilicate, and on the other hand, to the presence of carbonated and silicate minerals (Table 2).

Table 2. Chemical compositions of mixtures used in brick fabrication (%)

SiO ₂	Al ₂ O ₃	CaO	Fe ₂ O ₃	MgO	K ₂ O	TiO ₂	Na ₂ O	P ₂ O ₃	Fire loss mass at 1050°C
47.2	13.6	13.0	5.6	2.3	2,3	0.7	0.3	0.1	15.6

- The liquid limit and plasticity index of this brick's materials have corresponding values of 42.9% and 22.9%, respectively. By plotting these results on the Casagrande's plasticity chart [36], the brick falls within the range of soils with medium plasticity, indicating that a small amount of water can transform it from a solid to a liquid state.
- Based on the methylene blue test for specific surface area determination [37], this type of brick has a more important internal surface area compared to traditionally handmade bricks, which results in higher water adsorption and increased thermal and hydric-induced deformations.
- The apparent permeability and water vapor diffusion resistance factor were found to be very low compared to other building materials, highlighting the hygroscopic nature of the brick.

3.2. Experimental equipment

The resistivity meter utilized in this study was a Syscal Junior Switch-48, comprising a multiplexing system capable of managing up to 48 electrodes (2 sets of 24 electrodes) and a 100W power source (Figure 2). The resistivity meter can be connected to 4 electrodes for the standard measurement (2 injection electrodes and 2 reception electrodes) or to multiple electrodes for use in multi-electrode mode through the multiplexer.

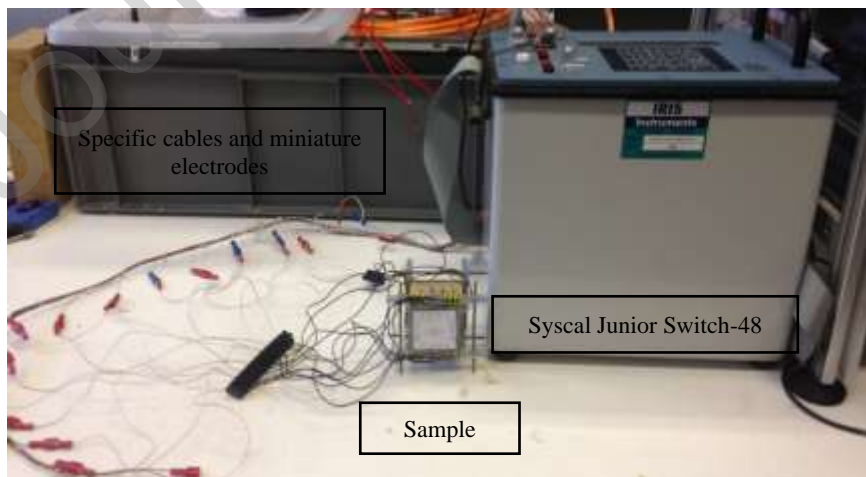


Figure 2. Experimental equipment

For materials possessing high electrical resistance, the achievable current intensity for injection purposes becomes considerably low, even with a maximum voltage of 400V. This intensity approaches the resolution limit in the standard configuration of the resistivity meter device. Consequently, the accuracy of current measurement becomes problematic. To address this issue, a

current divider module was installed, which reduced the injection range from 1250mA to 50mA. This modification resulted in an improved resolution from $10\mu\text{A}$ to $0.4\mu\text{A}$. In the 50mA mode, the intensity is thus divided by 25. Previous studies by Nguyen [38] and Hafsa et al. [30] have also utilized this device for measuring the resistivity of wood materials.

The electrodes for resistivity measurements in a semi-infinite medium in geophysics is not suitable for the scale of the samples investigated in this study, as they have a finite size of a few centimeters. Therefore, specific cables and miniature electrodes were fabricated to accommodate this requirement (Figure 2). The electrodes were fabricated by pouring a molten alloy, composed of 99.3% tin (Sn) and 0.7% copper (Cu), into pre-drilled cylindrical. This allowed for electrical cable connections to be made, as illustrated in Figure 3.

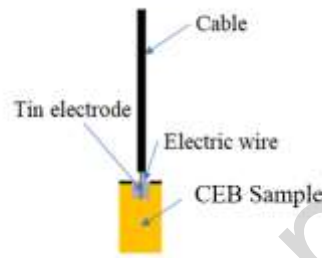


Figure 3. Deep-insertion electrode

3.3. Electrical Measurement

Standard mode measurement

The standard mode is a specific measurement technique that involves conducting measurements at four distinct points. In this study, the standard mode is applied to a brick sample with dimensions of $50 \times 40 \times 40 \text{mm}^3$ (named standard sample), which is obtained by cutting a full-sized brick. The purpose of reducing the brick size is to expedite the moisture diffusion experiment and thereby reduce the overall duration of the experiment. To facilitate the measurements, four cylindrical deep-insertion electrodes with a diameter of 2mm and a depth of 3mm strategically arranged at a spacing of 10mm, as illustrated in the Figure 4.

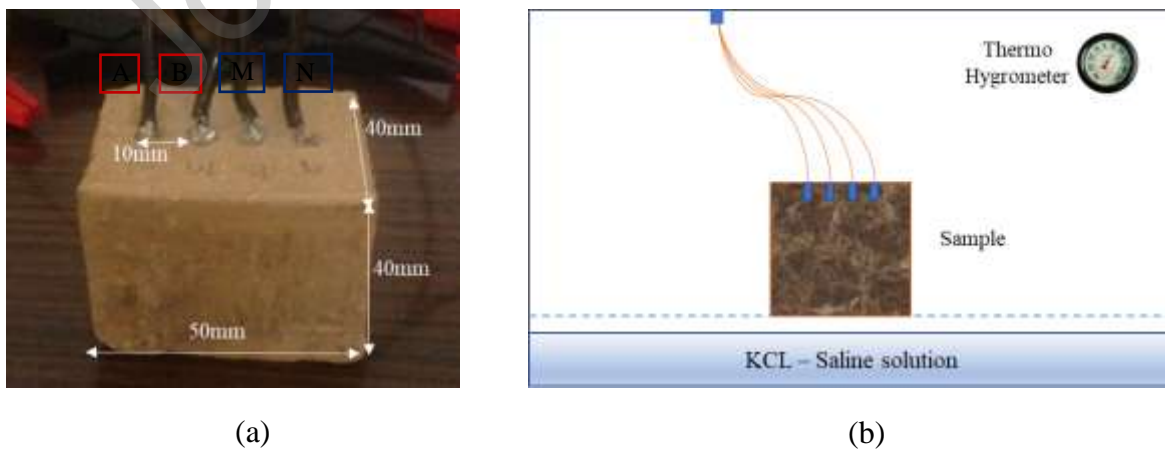


Figure 4. Standard sample (a) and hydric experimental setup (b)

The standard sample (Figure 4a) is subjected to different levels of relative humidity (RH) by being placed inside a desiccator (Figure 4b). The desiccator serves as an apparatus for regulating the

ambient environment, allowing for the establishment of specific conditions in terms of RH and temperature, which are determined by the amount of water and salt present. At each equilibrium state achieved by the standard sample corresponding to RH values of 100%, 70%, 60%, 50%, 40%, and 20%, electrical measurements are performed to evaluate its characteristics.

Comparing with the sample mass after drying, the corresponding moisture content for different RH was conducted in the laboratory and is presented in the Table 3.

Table 3. Moisture content of the standard sample

Relative humidity	20%	40%	50%	60%	70%	100%
Moisture Content	1.86%	2.90%	3.46%	4.32%	4.89%	9.48%

In the context of the standard mode measurement, the dipole-dipole configuration (Figure 1) is employed due to its capability to achieve a notably low level of electromagnetic interaction between the current and potential lines, while simultaneously ensuring a dense distribution of measurement points [38]. This electrical experiment is conducted utilizing two distinct injection modes, specifically employing injection currents of 1250mA and 50mA for each measurement.

Multiplexed quadrupoles measurements

In this study, two representative samples of equal dimensions, specifically measuring $50 \times 50 \times 50 \text{mm}^3$, were obtained by cutting full-sized bricks. These samples were carefully prepared and subjected to controlled environmental conditions in order to investigate the effects of different RH levels. One sample was exposed to 40% RH, while the other sample was exposed to a higher 70% RH.

The electrical resistivity measurements were carried out on the samples at a state of moisture equilibrium corresponding to each RH level. The moisture content of the samples was determined by calculating the mass of the dried samples, as obtained through drying procedures. The moisture content of the first sample was determined to be 2.5%, while the second sample exhibited a moisture content of 4.0%.

A total of 16 electrodes are carefully inserted around the perimeter of a designated symmetry plane within the sample. These electrodes are evenly spaced at intervals of 10mm, possess a depth of 3mm, and exhibit a diameter of 2mm. To ensure consistent and reliable contact between the metal electrodes and the sample, a specialized frame is meticulously prepared to securely hold the cables in place throughout the duration of the measurements (Figure 5).



Figure 5. Multiplexed quadrupoles measurements

The first series of quadrupoles involves deploying Dipole-Dipole configurations with different spacing around the perimeter of the section. The second type of quadrupoles involves crossing the sample with current lines and measuring the potential difference along a parallel line (Figure 6). The combination of two series of quadrupoles conducted on 16 electrodes resulted in 136 measured resistance values.

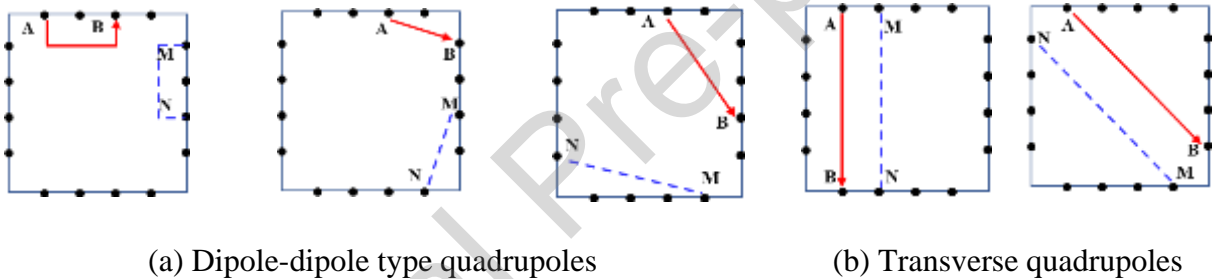


Figure 6. Examples of quadrupoles

Following the same approach as the 4-electrodes experiment, the multiplexer experiments utilized two different resistance measurement modes: 1250mA and 50mA.

4. Numeric model

The generalized Ohm's law and Fourier's law demonstrate a clear analogy between the behavior of electrical conduction and heat transfer in steady-state conditions [33]. There are correlations between electrical and thermal quantities, enabling the utilization of all heat transfer techniques provided by the Castem finite element code [39]. Finite element meshing involves two key aspects: the discretization of electrodes, which serve as both current injection points and potential measurement points, and the discretization of the sample volume.

In this study, the problem is symmetrical, involving a homogeneous environment with uniform resistivity. Given these conditions, it was determined that modeling half of the sample would be sufficient for the calculations. This approach simplifies the analysis while maintaining the accuracy of the results.

The current is applied as a uniform flux density on the upper surface of the electrode. The electrodes are constructed from a nearly infinitely conductive material with a resistivity of $\rho = 10^{-7} \Omega\text{m}$. The electrodes are modelled as cylinders with a length of 3mm and a diameter of 2mm. This cylinder allows the transfer of a current density, imposed on the electrode surface, towards the

electrode/CEB contact surface; the CEB in the vicinity of the electrode is modelled by a block that will connect to the overall volume of the sample. The next step involves implanting the electrodes into the sample: 4 in-line electrodes spaced 10mm apart for the standard sample with dimensions of 50x40x40mm³, and 16 electrodes spaced 10mm apart and arranged in a perimeter layout for the sample with dimensions of 95x95x95mm³ (Figure 7).

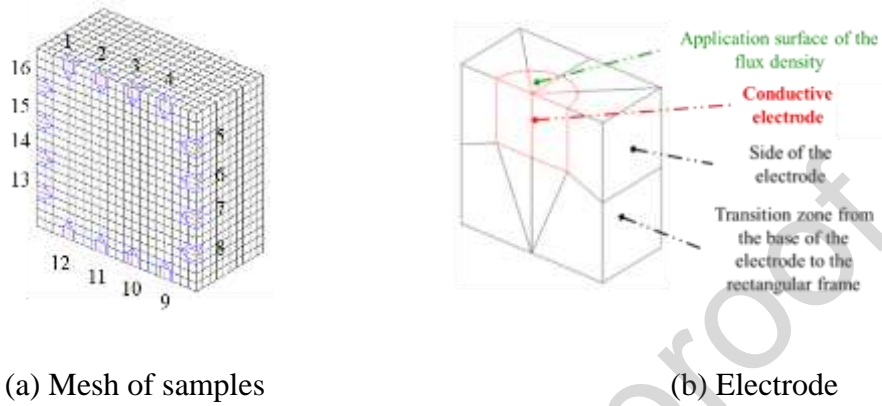


Figure 7. Mesh of samples and electrode

The measurement principle is based on the user's selection of a desired potential difference, ΔV_{MN} , which determines the value of the injection current I_{AB} . The voltage and injection current automatically adjust accordingly. The relationship follows a linear Ohm's law, where the resistance value remains constant regardless of the injected potential or current. Consequently, the model employs a fixed injection current of 1A. The numeric model has the capability to calculate the numerical values of resistance for any electrode configurations, given arbitrary sample dimensions and resistivity.

5. Results and Discussion

Standard mode measurement results

The measurement results for the standard sample using the Dipole-Dipole configuration are presented in Table 4. It can be observed that the $\frac{\Delta V_{MN}}{I_{AB}}$ values obtained vary logarithmically with the moisture content of the test sample, showing a trend where lower humidity results in higher $\frac{\Delta V_{MN}}{I_{AB}}$ values. Measurements using the 1250 mA mode could not be performed with a RH below 40%, corresponding to a sample moisture content of 2.9%. At RH50%, this measurement is still feasible and yields a $\frac{\Delta V_{MN}}{I_{AB}}$ value equivalent to that of the 50mA mode.

Table 4. The measurement results of $\frac{\Delta V_{MN}}{I_{AB}}$ for the standard sample

RH (%)	Moisture content (%)	50mA Mode (Ω)	1250mA Mode (Ω)	Deviation between the two modes
20	1.86	12007.25	x	

40	2.90	1363.00	x	
50	3.46	155.50	151.00	2.89%
60	4.32	115.25	126.69	9.93%
70	4.89	92.75	87.03	6.17%
100	9.48	49.86	57.55	15.43%

Note: an 'x' mark means the measurement could not be performed.

In considering the numerical model of the standard sample (which has the same dimensions and arrangement of 4 electrodes as in the experiment as shown as Figure 4), it is assumed that the standard sample has a unitary resistivity. Corresponding accurately to the experimental equipment setup, the numerical model yields a result for the $\left(\frac{\Delta V_{MN}}{I_{AB}}\right)_{num}$ of 3.11Ω .

The sample in the experiment reaches saturation moisture content, hence, it is hypothesized to have homogeneous resistivity. In accordance with the linear nature of Ohm's law, when considering a sample with identical geometric dimensions and electrical experimental setup, the true resistivity of the sample can be inferred using the formula presented below:

$$\rho = \frac{\left(\frac{\Delta V_{MN}}{I_{AB}}\right)_{exp}}{\left(\frac{\Delta V_{MN}}{I_{AB}}\right)_{num}} \quad (4)$$

$$\left(\frac{\Delta V_{MN}}{I_{AB}}\right)_{exp} : \frac{\Delta V_{MN}}{I_{AB}} \text{ measured.}$$

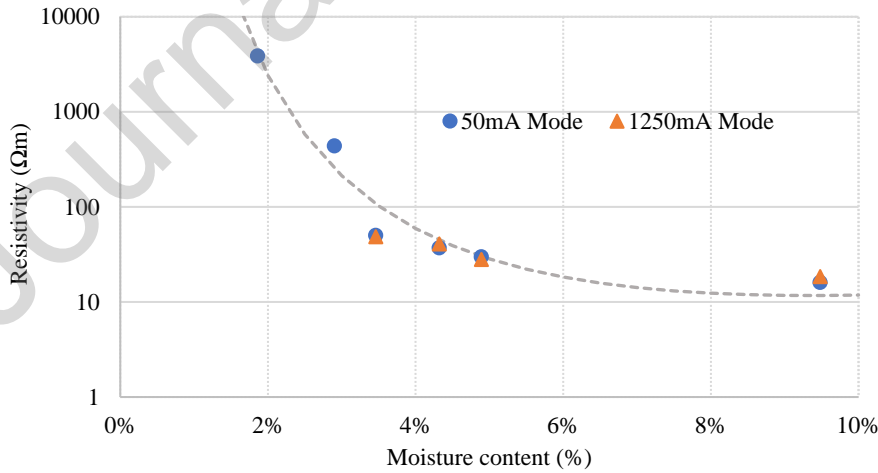


Figure 8. The variation of resistivity with moisture content

The results calculated using formula 4, showing the actual resistivity of the standard CEB sample, are presented in Figure 8. It is noticeable that the calculated resistivity of CEB varies with moisture content. The measured electrical resistivity varied from $12.4\Omega m$ at 9.48% moisture content to $3350\Omega m$ at 1.86% moisture content.

The resistivity results of the test sample in Figure 8 indicate that the two measurement modes, 1250mA and 50mA, yield fairly similar resistivity values on a logarithmic scale. The 50mA mode

demonstrates effectiveness in conducting measurements for CEB samples with lower moisture content (below 3%).

Multiplexed quadrupoles measurements

The numeric model developed in this study allows for the determination of resistance values for various quadrupole configurations established in a finite medium with arbitrary resistivity. For the case of multi-electrode experimental setup with sample and electrode arrangement as shown in Figure 6, assuming a homogeneous sample with unit resistivity values, the numerical model can compute 136 values of $\frac{\Delta V_{MN}}{I_{AB}}$, as depicted in Figure 9. The observed variations in resistance values demonstrate the sensitivity of the resistance measurements to changes in the quadrupole configuration.

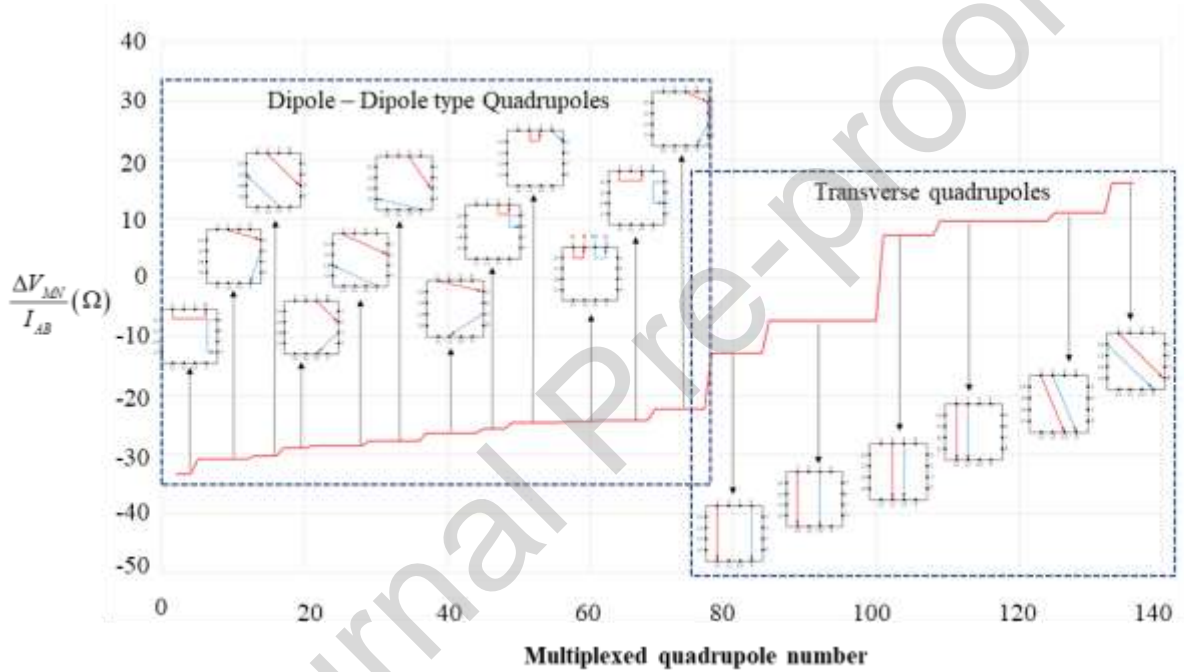


Figure 9. The modelled values of the $\frac{\Delta V_{MN}}{I_{AB}}$ ratio for the test sample with unit resistivity are organized in ascending order

The $\frac{\Delta V_{MN}}{I_{AB}}$ modelling values with a unitary resistivity field, as depicted in Figure 9, indicate that the transverse quadrupole group yields larger measured $\frac{\Delta V_{MN}}{I_{AB}}$ values compared to the Dipole-Dipole type quadrupole group.

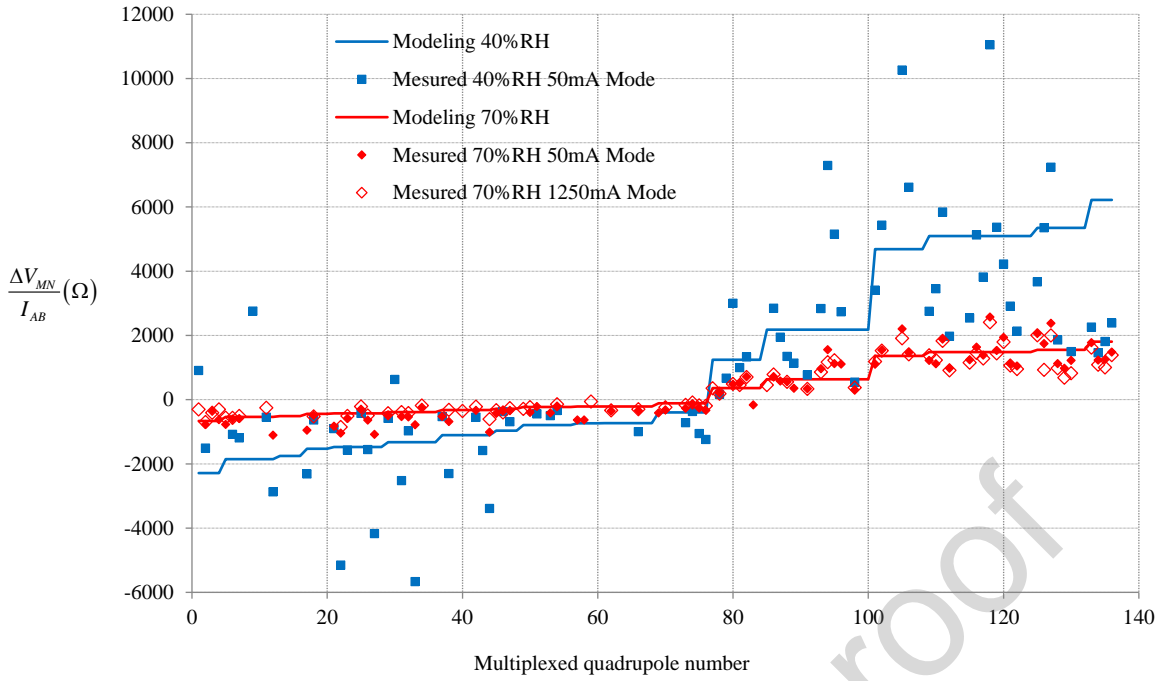


Figure 10. The results of the measurements and modelling of $\frac{\Delta V_{MN}}{I_{AB}}$

The experimental results conducted on two test samples are also presented in Figure 10. As discussed above, the experiments were performed in both modes: 1250mA and 50mA. The experimental results allow for the following conclusions to be drawn:

- At lower RH, corresponding to lower moisture content of the test sample, the measured resistance values are higher, indicating larger variations between measurements.
- Similarly, to the case of using 4 electrodes discussed earlier, at a RH of 40%, the 1250mA mode was unable to produce reliable results. This confirms that the 1250mA mode is not suitable for measuring the resistance of the brick with a relative humidity below 40%, corresponding to a brick moisture content of 2.5-3%.
- The 50mA measurement mode is capable of measuring the resistance of the brick at a moisture content of approximately 2.5%. However, the deviations among the measured resistance values also suggest that a higher-powered measurement mode may provide more accurate results.

In this scenario, where the sample exhibits uniform resistivity, a comparative analysis between the experimental findings and the model, as delineated in Equation 4, facilitates the determination of the CEB sample's true resistivity derived from each $\frac{\Delta V_{MN}}{I_{AB}}$ value. For heightened precision, the entirety of the 136 values of $\frac{\Delta V_{MN}}{I_{AB}}$ is employed. The modelling of the $\frac{\Delta V_{MN}}{I_{AB}}$ ratio is established through an error minimization approach against experimental values. With ρ representing the sample's resistivity, the least squares objective function, bridging the measured and modelled data, is methodically computed.

$$f = \sqrt{\frac{\sum_{i=1}^N \left[\left(\frac{\Delta V_{MN}}{I_{AB}} \right)_{\text{exp}}^i - \rho \cdot \left(\frac{\Delta V_{MN}}{I_{AB}} \right)_{\text{num}}^i \right]^2}{N}} \quad (5)$$

$\left(\frac{\Delta V_{MN}}{I_{AB}} \right)_{\text{exp}}^i$: $\frac{\Delta V_{MN}}{I_{AB}}$ measured at the i-th quadrupole.

$\left(\frac{\Delta V_{MN}}{I_{AB}} \right)_{\text{num}}^i$: $\frac{\Delta V_{MN}}{I_{AB}}$ modelling at the i-th quadrupole in a sample with a resistivity of 1.

N : Number of quadrupoles.

The homogeneous resistivity of the cube in a perimeter layout is determined by minimizing this function using Excel's Solver. The calculated resistivity values corresponding to RH40% and RH70% have been added to the chart depicting the variation of resistivity with moisture content of the standard sample, as shown in the Figure 11. These results are incorporated into the graph and show a good fit with the logarithmic curve obtained from the standard test.

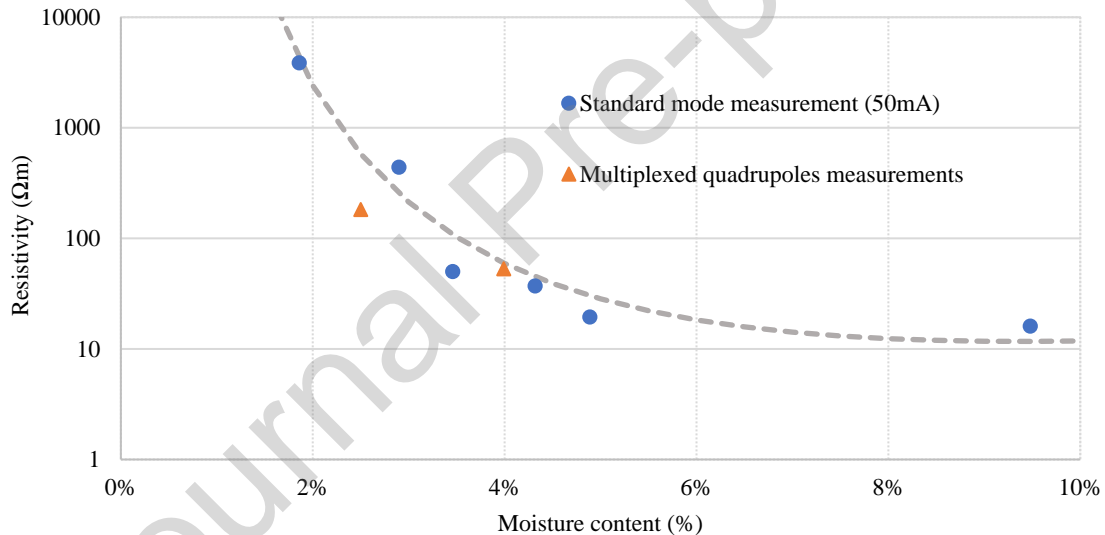


Figure 11. The variation of resistivity in relation to the moisture content of both the standard and multiplexed test samples

This research primarily focuses on exploring the potential enhancements of resistivity measuring devices in geotechnical applications for CEB usage. The findings reveal that, in the 50mA mode, the instrument is capable of conducting measurements at moisture content above 2.9%. It is anticipated that at higher humidity levels, the measurement accuracy could be significantly improved. This forms a foundational basis for future studies aimed at investigating the variations in moisture content within CEB structures through electrical methodologies.

6. Conclusion and perspectives

The present article represents one of the initial studies on the use of electrical methods in geotechnical engineering for investigating moisture content in CEB. The novelty of this approach lies in the application of electrical resistivity tomography techniques, traditionally used in geophysics, to the field of building material assessment. The resistivity meter was upgraded in terms

of power capacity and modifications were made to some components, such as cables and electrodes, to suit CEB applications. This research demonstrates the feasibility of using electrical resistivity method to non-destructively determine moisture content in CEB.

In the standard measurement mode, the results reveal clear logarithmic correlations between moisture content and electrical resistivity of the bricks, enabling moisture levels to be inferred from resistivity values. The measured electrical resistivity varied from $12.4\Omega\text{m}$ at 9.48% moisture content to $3350\Omega\text{m}$ at 1.86% moisture content, demonstrating the method's sensitivity across a wide range of moisture levels. While the 1250mA mode exhibited problems below 2.9% moisture content, switching to a more sensitive 50mA mode improved results, allowing determination down to 1.86% moisture content. However, the measured results exhibited substantial deviations even when conducted with the same type of quadrupole.

The multiplexed electrode measurements demonstrated capability to discern moisture levels from resistivity contrasts down to 2.5% moisture content using the 50mA mode. Calculated resistivity values showed good agreement with the experimental trend. Larger discrepancies occurred at lower moistures between measured and calculated resistances, although measurements followed expected resistance variations.

In summary, the electrical resistivity method shows promise for non-destructive determination of moisture content in CEB under diffusion-based moisture ingress conditions. For typical resistivity meters, effective assessment of CEB, moisture content is achieved down to approximately 3% moisture levels. It is anticipated that at higher moisture content, this approach will demonstrate even greater efficacy, especially when deployed to probe the presence of free water within the CEB specimens. The technique exhibits aptitude for identification of elevated moisture magnitudes and free water occurrence. Additionally, the multiplexed electrode arrangements exhibit potential for internal moisture distribution mapping within the CEBs structure. This approach opens up prospects for creating new non-destructive methods to monitor moisture in structures using CEBs as well as other types of earth-based materials. By bridging the gap between geophysical surveying and construction material analysis, this research paves the way for innovative monitoring solutions in sustainable building practices and heritage conservation efforts.

Additional efforts are requisite to broaden the experimentally-examined moisture content spectrum, thereby facilitating comprehensive characterization of the resistivity- moisture content relationship across more expansive humidity variants. Rigorous comparative analyses benchmarked against conventionally-employed techniques would be beneficial to further validate the electrical resistivity approach proposed herein. Methodical exploration of alternative electrode arrangements and inter-electrode spacings should be undertaken to potentially enhance measurement sensitivities and expand detection thresholds to lower moisture content. Moreover, engineering automated, multi-electrode scanning systems could unlock capability for expedited internal moisture mapping within earthen construction components. Such systems may be coupled with numerical modeling to reconstruct three-dimensional moisture content profiles. Overall, refinement of this electrical resistivity technology offers much promise to aid ongoing adoption of sustainable construction solutions harnessed from locally-available earthen resources. The technique represents a practical, non-destructive means to monitor critical moisture exposure in earth-based masonry structures.

References

- [1] H. Houben and H. Guillaud, *Earth construction : a comprehensive guide*. in Earth construction series. Warwickshire: Practical Action Publishing, 2008.
- [2] J. C. Morel, A. Mesbah, M. Oggero, and P. Walker, “Building houses with local materials: means to drastically reduce the environmental impact of construction,” *Building and Environment*, vol. 36, no. 10, pp. 1119–1126, Dec. 2001, doi: 10.1016/S0360-1323(00)00054-8.
- [3] D. Gallipoli, A. W. Bruno, C. Perlot, and J. Mendes, “A geotechnical perspective of raw earth building,” *Acta Geotechnica*, vol. 12, no. 3, pp. 463–478, Jun. 2017, doi: 10.1007/s11440-016-0521-1.
- [4] R. Abid, N. Kamoun, F. Jamoussi, and H. El Feki, “Fabrication and properties of compressed earth brick from local Tunisian raw materials,” *Boletín de la Sociedad Española de Cerámica y Vidrio*, vol. 61, no. 5, pp. 397–407, Sep. 2022, doi: 10.1016/j.bsecv.2021.02.001.
- [5] J. Saliba, A. Schultz, J. Moye, and K. Pistol, “Mechanical characterization and durability of earth blocks,” *Materials Today: Proceedings*, Jul. 2023, doi: 10.1016/j.matpr.2023.06.165.
- [6] M. Gomaa, S. Schade, D. W. Bao, and Y. M. Xie, “Automation in rammed earth construction for industry 4.0: Precedent work, current progress and future prospect,” *Journal of Cleaner Production*, vol. 398, p. 136569, Apr. 2023, doi: 10.1016/j.jclepro.2023.136569.
- [7] D. Allinson and M. Hall, “Hygrothermal analysis of a stabilised rammed earth test building in the UK,” *Energy and Buildings*, vol. 42, no. 6, pp. 845–852, Jun. 2010, doi: 10.1016/j.enbuild.2009.12.005.
- [8] B. V. V. Reddy, “Earthen Materials and Earthen Structures,” in *Compressed Earth Block & Rammed Earth Structures*, B. V. V. Reddy, Ed., Singapore: Springer Nature Singapore, 2022, pp. 3–55. doi: 10.1007/978-981-16-7877-6_1.
- [9] H. Niroumand, R. Akbari, K. Khanlari, A. B. Gültekin, and J. A. Barcelo, “A Systematic Literature Review of Rammed Earth Walls,” *Soil Mechanics and Foundation Engineering*, vol. 58, no. 4, pp. 295–301, Sep. 2021, doi: 10.1007/s11204-021-09742-y.
- [10] F. Pacheco-Torgal and S. Jalali, “Earth construction: Lessons from the past for future eco-efficient construction,” *Construction and Building Materials*, vol. 29, pp. 512–519, Apr. 2012, doi: 10.1016/j.conbuildmat.2011.10.054.
- [11] G. Ruiz, X. Zhang, W. F. Edris, I. Cañas, and L. Garijo, “A comprehensive study of mechanical properties of compressed earth blocks,” *Construction and Building Materials*, vol. 176, pp. 566–572, Jul. 2018, doi: 10.1016/j.conbuildmat.2018.05.077.
- [12] J.-C. Morel, A. Pkla, and P. Walker, “Compressive strength testing of compressed earth blocks,” *Construction and Building Materials*, vol. 21, no. 2, pp. 303–309, Feb. 2007, doi: 10.1016/j.conbuildmat.2005.08.021.
- [13] J. C. Morel and A. Pkla, “A model to measure compressive strength of compressed earth blocks with the ‘3 points bending test,’” *Construction and Building Materials*, vol. 16, no. 5, pp. 303–310, Jul. 2002, doi: 10.1016/S0950-0618(02)00023-5.
- [14] P. Maillard and J. E. Aubert, “Effects of the anisotropy of extruded earth bricks on their hygrothermal properties,” *Construction and Building Materials*, vol. 63, pp. 56–61, Jul. 2014, doi: 10.1016/j.conbuildmat.2014.04.001.
- [15] L. Zhang, L. Yang, B. P. Jelle, Y. Wang, and A. Gustavsen, “Hygrothermal properties of compressed earthen bricks,” *Construction and Building Materials*, vol. 162, pp. 576–583, Feb. 2018, doi: 10.1016/j.conbuildmat.2017.11.163.
- [16] M. Hall and D. Allinson, “Analysis of the hygrothermal functional properties of stabilised rammed earth materials,” *Building and Environment*, vol. 44, no. 9, pp. 1935–1942, Sep. 2009, doi: 10.1016/j.buildenv.2009.01.007.

- [17] H. Cagnon, J. E. Aubert, M. Coutand, and C. Magniont, “Hygrothermal properties of earth bricks,” *Energy and Buildings*, vol. 80, pp. 208–217, Sep. 2014, doi: 10.1016/j.enbuild.2014.05.024.
- [18] F. Champiré, A. Fabbri, J.-C. Morel, H. Wong, and F. McGregor, “Impact of relative humidity on the mechanical behavior of compacted earth as a building material,” *Construction and Building Materials*, vol. 110, pp. 70–78, May 2016, doi: 10.1016/j.conbuildmat.2016.01.027.
- [19] L. Laou, L. Ulmet, S. Yotte, J.-E. Aubert, and P. Maillard, “Simulation of the Hygro-Thermo-Mechanical Behavior of Earth Brick Walls in Their Environment,” *Buildings*, vol. 13, no. 12, p. 3061, Dec. 2023, doi: 10.3390/buildings13123061.
- [20] L. Laou, J. E. Aubert, S. Yotte, P. Maillard, and L. Ulmet, “Hygroscopic and mechanical behaviour of earth bricks,” *Materials and Structures*, vol. 54, no. 3, p. 116, May 2021, doi: 10.1617/s11527-021-01701-1.
- [21] D. Maskell, A. Heath, and P. Walker, “Laboratory scale testing of extruded earth masonry units,” *Materials & Design*, vol. 45, pp. 359–364, Mar. 2013, doi: 10.1016/j.matdes.2012.09.008.
- [22] B. Taallah, A. Guettala, S. Guettala, and A. Kriker, “Mechanical properties and hygroscopicity behavior of compressed earth block filled by date palm fibers,” *Construction and Building Materials*, vol. 59, pp. 161–168, May 2014, doi: 10.1016/j.conbuildmat.2014.02.058.
- [23] R. A. Tchouateu Kamwa *et al.*, “Stabilization of compressed earth blocks (CEB) by pozzolana based phosphate geopolymer binder: Physico-mechanical and microstructural investigations,” *Cleaner Materials*, vol. 4, p. 100062, Jun. 2022, doi: 10.1016/j.clema.2022.100062.
- [24] Lamyaa Laou, “Evaluation du comportement mécanique sous sollicitations thermohydriques d’un mur multimatériaux (bois, terre crue, liants minéraux) lors de sa construction et de son utilisation,” Université de Limoges, France, 2017.
- [25] W. Edris and M. Tamimi, “Potential Utilization of Oil Shale as a Stabilizing Material for Compressed Earth Block,” *Frontiers in Built Environment*, vol. 22, Jun. 2023, doi: 10.3389/fbuil.2023.1199744.
- [26] M. Ben Mansour, E. Ogam, Z. E. A. Fellah, A. Soukaina Cherif, A. Jelidi, and S. Ben Jabrallah, “Characterization of compressed earth blocks using low frequency guided acoustic waves,” *The Journal of the Acoustical Society of America*, vol. 139, no. 5, pp. 2551–2560, May 2016, doi: 10.1121/1.4948573.
- [27] E. Bernat-Maso, E. Teneva, C. Escrig, and L. Gil, “Ultrasound transmission method to assess raw earthen materials,” *Construction and Building Materials*, vol. 156, pp. 555–564, Dec. 2017, doi: 10.1016/j.conbuildmat.2017.09.012.
- [28] N. Sathiparan, W. G. B. S. Jayasundara, K. S. D. Samarakoon, and B. Banujan, “Prediction of characteristics of cement stabilized earth blocks using non-destructive testing: Ultrasonic pulse velocity and electrical resistivity,” *Materialia*, vol. 29, p. 101794, Jun. 2023, doi: 10.1016/j.mtla.2023.101794.
- [29] E. R. Teixeira *et al.*, “Mechanical and Thermal Performance Characterisation of Compressed Earth Blocks,” *Energies*, vol. 13, no. 11, p. 2978, Jun. 2020, doi: 10.3390/en13112978.
- [30] W. Hafsa *et al.*, “Assessment of moisture content profile in Douglas-fir wood using electrical resistivity-based tomography,” *Construction and Building Materials*, vol. 366, p. 130193, Feb. 2023, doi: 10.1016/j.conbuildmat.2022.130193.
- [31] J. D. Ducut *et al.*, “A Review of Electrical Resistivity Tomography Applications in Underground Imaging and Object Detection,” *Displays*, vol. 73, p. 102208, Jul. 2022, doi: 10.1016/j.displa.2022.102208.
- [32] A. Neyamadpour, W. A. T. Wan Abdullah, and S. Taib, “Use of four-electrode arrays in three-dimensional electrical resistivity imaging survey,” *Studia Geophysica et Geodaetica*, vol. 54, no. 2, pp. 299–311, Apr. 2010, doi: 10.1007/s11200-010-0016-8.

- [33] P. Rochowski and G. Pontrelli, “Mass diffusion in multi-layer systems: an electrical analogue modelling approach,” *Computers in Biology and Medicine*, vol. 148, p. 105774, Sep. 2022, doi: 10.1016/j.combiomed.2022.105774.
- [34] U. Singh and P. Sharma, “Study on geometric factor and sensitivity of subsurface for different electrical resistivity Tomography Arrays,” *Arabian Journal of Geosciences*, vol. 15, p. 560, Apr. 2022, doi: 10.1007/s12517-022-09844-3.
- [35] Q.-B. Bui and J.-C. Morel, “Assessing the anisotropy of rammed earth,” *Construction and Building Materials*, vol. 23, no. 9, pp. 3005–3011, Sep. 2009, doi: 10.1016/j.conbuildmat.2009.04.011.
- [36] A. Shakoor, “Atterberg Limits,” in *Encyclopedia of Engineering Geology*, P. T. Bobrowsky and B. Marker, Eds., Cham: Springer International Publishing, 2018, pp. 44–47. doi: 10.1007/978-3-319-73568-9_22.
- [37] P. Arab, T. Araujo, and O. Pejon, “Identification of clay minerals in mixtures subjected to differential thermal and thermogravimetry analyses and methylene blue adsorption tests,” *Applied Clay Science*, vol. 114, pp. 133–140, Sep. 2015, doi: 10.1016/j.clay.2015.05.020.
- [38] N. Tuan Anh, “Approches expérimentales et numériques pour l’étude des transferts hygroscopiques dans le bois,” Université de Limoges, 2014.
- [39] A. Combescure, A. Hoffmann, and P. Pasquet, “The CASTEM Finite Element System,” in *Finite Element Systems: A Handbook*, C. A. Brebbia, Ed., Berlin, Heidelberg: Springer Berlin Heidelberg, 1982, pp. 115–125. doi: 10.1007/978-3-662-07229-5_8.

Declaration of Competing Interest

The authors declare that they have no known competing financial interests or personal relationships that could have appeared to influence the work reported in this paper.